DOI: 10.1002/cphc.200600190

# Characterization of $O_2$–$CeO_2$ Interactions Using In Situ Raman Spectroscopy and First-Principle Calculations

Y. M. Choi,[a] Harry Abernathy,[a] Hsin-Tsung Chen,[b] M. C. Lin,[b, c] and Meilin Liu*[a]

*Interactions between $O_2$ and $CeO_2$ are examined experimentally using in situ Raman spectroscopy and theoretically using density-functional slab-model calculations. Two distinct oxygen bands appear at 825 and 1131 $cm^{-1}$, corresponding to peroxo- and superoxo-like species, respectively, when partially reduced $CeO_2$ is exposed to 10% $O_2$. Periodic density-functional theory (DFT) calculations aid the interpretation of spectroscopic observations and provide energetic and geometric information for the dioxygen species adsorbed on $CeO_2$. The $O_2$ adsorption energies on unreduced $CeO_2$ surfaces are endothermic ($0.91 < \Delta E_{ads} < 0.98$ eV), while those on reduced surfaces are exothermic ($-4.0 < \Delta E_{ads} < -0.9$ eV), depending on other relevant surface processes such as chemisorption and diffusion into the bulk. Partial reduction of surface $Ce^{4+}$ to $Ce^{3+}$ (together with formation of oxygen vacancies) alters geometrical parameters and, accordingly, leads to a shift in the vibrational frequencies of adsorbed oxygen species compared to those on unreduced $CeO_2$. Moreover, the location of oxygen vacancies affects the formation and subsequent dissociation of oxygen species on the surfaces. DFT predictions of the energetics support the experimental observation that the reduced surfaces are energetically more favorable than the unreduced surfaces for oxygen adsorption and reduction.*

## 1. Introduction

Cerium oxide ($CeO_2$) has been extensively used for various catalytic and electrocatalytic applications such as purification of automobile exhaust gases in three-way catalysts[1] and direct production of hydrogen from methanol.[2,3] In addition, rare-earth-doped ceria electrolytes (e.g. gadolinia-doped ceria, GDC) have been used to replace yttria-stabilized zirconia (YSZ) for lower-temperature solid-oxide fuel cells (SOFCs).[4] For these applications, the presence of oxygen vacancies within $CeO_2$ and the oxidation state of Ce cations play a vital role in determining the catalytic and transport properties of the materials.[3] Understanding the detailed interaction between oxygen and $CeO_2$ is important to the development of high-performance ceria-based catalysts/electrocatalysts and electrolytes. In many cases, however, mechanistic details are difficult to observe directly from experiments due either to the inherent inaccessibility of the processes or to the complexity of the gas–surface interactions. It thus becomes imperative to couple experimental measurements with quantum-chemical calculations to fully elucidate $O_2$–$CeO_2$ interactions. To date, however, periodic density-functional theory (DFT) calculations have not yet been applied to the interpretation the spectroscopy of $O_2$–$CeO_2$ interactions, although $CeO_2$ has been extensively studied.[5–7] Herein we report on the characterization of adsorbed oxygen species on $CeO_2$ using in situ Raman spectroscopy as well as the interpretation of the Raman spectra by DFT calculations. The $O_2$–$CeO_2$ interactions are examined in terms of the energetic stability of adsorbed dioxygen species. We further examine how oxygen vacancies and their crystallographic locations influence the catalytic activity of different sites for oxygen adsorption and dissociation (similar to that of methanol).[3] In particular, we estimate the vibrational frequencies of optimized structures of adsorbed oxygen species, establishing the scientific basis for the interpretation of vibrational spectra.

## Experimental and Computational Methods

Details of the experimental set up and techniques are described elsewhere (see Figure S1 in the Supporting Information).[8] All Raman measurements were taken by a Raman microscope (Renishaw RM1000) with a 1800-line $mm^{-1}$ diffraction grating and a charge-coupled device (CCD) detector using a 488 nm Ar-ion laser source (Melles Griot). Cerium oxide powder (Sigma–Aldrich, average particle size = 10–20 nm, ≈0.3 g) was pressed into a pellet of 10 mm diameter, placed inside the atmosphere- and temperature-controlled sample chamber (special order, Harrick Scientific), and purged for four hours with Ar (Airgas, UHP grade) at approximately

[a] *Dr. Y. M. Choi, H. Abernathy, Prof. Dr. M. Liu*
*Center for Innovative Fuel Cell and Battery Technologies*
*School of Materials Science and Engineering*
*Georgia Institute of Technology, Atlanta, GA 30332 (USA)*
*Fax: (+1) 404-894-9140*
*E-mail: meilin.liu@mse.gatech.edu*

[b] *Dr. H.-T. Chen, Prof. Dr. M. C. Lin*
*Department of Chemistry, Emory University*
*1515 Dickey Drive, Atlanta, GA 30322 (USA)*

[c] *Prof. Dr. M. C. Lin*
*Center for Interdisciplinary Molecular Science*
*National Chiao Tung University, Hsinchu, 30010 (Taiwan)*

*Supporting information for this article is available on the WWW under http://www.chemphyschem.org or from the author.*

  

673 K. The sample was then reduced through exposure to 5% $H_2$ balanced with Ar at the same temperature. The sample was cooled to room temperature under a flow of Ar before exposing the pellet to 10% $O_2$ balanced with Ar (Airgas, UHP grade). The surface-treatment process for partial reduction plays a significant role in the observation of adsorbed species, especially peroxo-like species.[5,9,10] According to Henderson et al.[11] approximately 40% of the $Ce^{4+}$ ions are reduced to $Ce^{3+}$ ions at 773 K. Isotope-substitution experiments with a 10% $^{18}O_2/^{16}O_2$ mixture balanced with Ar (Isotec, >92% $^{18}O_2$) were carried out to verify surface-adsorbed oxygen species.

To predict the interactions between $O_2$ and a cubic fluorite $CeO_2$ surface, we applied periodic DFT methods for electronic-structure calculations using the Vienna ab initio simulation package (VASP)[12] with the projector augmented wave (PAW)[13] method on a nine-layer super-cell that consists of 6 Ce and 12 O atoms, as shown in Figure 1a. To interpret the experimental observations fully using the polycrystalline $CeO_2$ powder, one needs to consider all possible surface planes since surface planes are linked to other types of facets (see Figure 1b). However, herein we examined only the $CeO_2$(111) surface to characterize the interactions between the

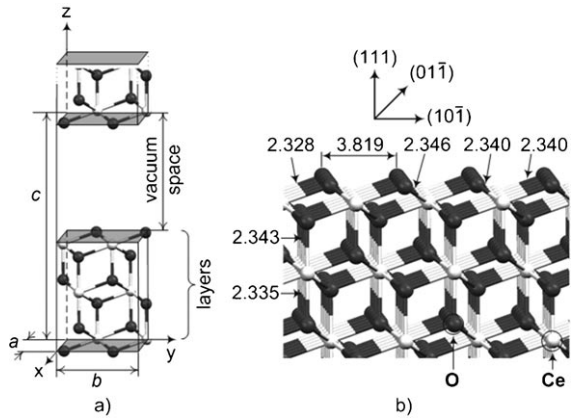


**Figure 1.** a) Surface model with nine layers for the $O_2$–$CeO_2$(111) interactions. b) Side view of the optimized bulk structure of $CeO_2$. Ce and oxygen ions are in white and in black, respectively. Bond lengths are in Å.

$O_2$ and the $CeO_2$(111) surface because it was reported that $CeO_2$-(111) is energetically the most stable[7,14] among the low-index $CeO_2$(111), (110), and (100) surfaces. Previous studies[7] suggested that a nine-layer surface model was sufficient for the $CeO_2$(111) surface calculations. As shown in Figure 1b, the (111) surface is composed of O—Ce–O stacks. All the calculations were carried out by relaxing the adsorbed oxygen molecule and the three top layers of the $CeO_2$(111) surface. The unrelaxed layers were set to the estimated bulk parameters. The exchange and correlation energies were described by the generalized gradient approximation (GGA) using the Perdew–Wang (PW91) functional. The calculations were carried out using (6×6×6) and (6×6×1) Monkhorst–Pack mesh **k**-points for bulk and surface calculations, respectively, and with a 400 eV cut-off energy, which allows convergence to 0.01 eV in the total energy. Both the cut-off energy and the **k**-point mesh have been shown to be sufficient for bulk $CeO_2$,[14] and the conditions were employed to carry out surface calculations for the $O_2$–$CeO_2$ interaction study with a vacuum spacing greater than 15 Å.

We calculated the relative energies according to Equation (1):

$$\Delta E = E[\text{slab} + O_2] - E[\text{slab}] - E[O_2] \quad (1)$$

where $E$[slab+$O_2$], $E$[slab], and $E$[$O_2$] are the calculated electronic energies of adsorbed oxygen species on the $CeO_2$ surface, the bare $CeO_2$ surface, and a spin-polarized oxygen molecule, respectively. $E$[$O_2$] represents the energy of a triplet gas-phase oxygen molecule with two unpaired electrons. According to the periodic DFT studies of Yang et al.,[7] the magnetic effect for $CeO_2$(111) using spin-polarization calculations is insignificant for adsorption energies and geometries; we have thus carried out the surface calculations with non-spin-polarization methods. We have also examined how the defect chemistry of $CeO_2$ affects the geometries and energetics by introducing oxygen vacancies, as will be discussed in detail in the following section. The vibrational frequencies of the adsorbed $O_2$ species on both unreduced and reduced $CeO_2$(111) surfaces were calculated by displacing only the adsorbed species. Partial charges of adsorbed oxygen species were also calculated using the Bader program.[15]

## 2. Results and Discussion

### 2.1. Adsorption of Oxygen Species on Unreduced and Reduced $CeO_2$ Surfaces

Depicted in Scheme 1 are visualization schemes for the $O_2$–$CeO_2$ interactions. The interaction of $O_2$ with unreduced $CeO_2$ produces various surface species such as side-on, end-on, and non-planar and planar bridging configurations (see Scheme 1a),[5] which are assigned to superoxo- or peroxo-like species. However, as illustrated in Scheme 1b, for a partially reduced $CeO_2$ surface, due to the presence of doubly charged oxygen vacancies ($\mathbf{V_O}^{\cdot\cdot}$), the geometries of the adsorbed oxygen species, especially at or near reduced cerium cations ($Ce^{3+}$), may be different from those on the unreduced surface. After molecular adsorption, subsequent incorporation of the adsorbed oxygen species into the bulk can occur to satisfy charge neutrality, bringing about oxygen-ion conduction.[16] Possible stepwise elementary steps involved in oxygen reduction (or evolution) at $CeO_2$ surfaces with oxygen vacancies are shown in Scheme 1c.[17] Molecular oxygen either reduces to superoxo- or peroxo-like oxygen ($O^-_{2(s)}$ or $O^{2-}_{2(s)}$, respectively), depending on the nature of the surfaces, followed by dissociation to monatomic ions $O^-_{(s)}$. The monatomic oxygen ion $O^-_{(ad)}$ then either reduces to $O^{2-}_{(ad)}$ followed by combination with an oxygen vacancy or combines directly with an electron and an oxygen vacancy.

### 2.2. Analysis of the Experimental Data

Shown in Figure 2a is a typical Raman spectrum for a fully oxidized $CeO_2$ sample at 298 K in 10% $O_2$. The bands at 465 and 1174 $cm^{-1}$ are attributable to typical first- and second-order phonon modes, respectively, for the cubic fluorite surface.[5,18] Figure 2b displays a Raman spectrum of the reduced ceria sample before and after exposure to an oxygen-containing atmosphere (10% $^{16}O_2$ or 10% $^{18}O_2$ in Ar). The intensity and presence of the peaks depend on the temperature of the sample and the effectiveness of the surface treatment used, similar to in previous works.[5,9,10] It is noted that, according to an X-ray photoelectron spectroscopy (XPS) study by Siokou and Nix,[19] the surface-treatment oxidation process cannot fully oxidize

  

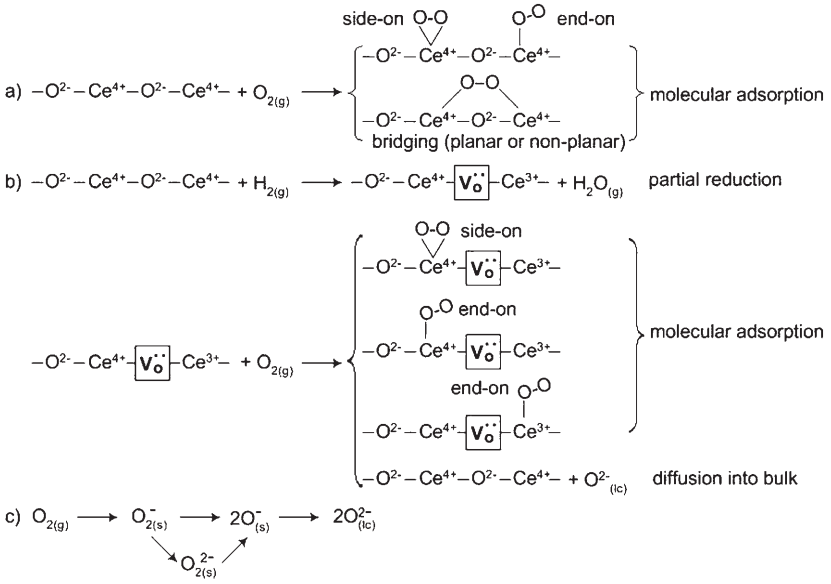


**Scheme 1.** Oxygen adsorption on a) an unreduced $CeO_2$ surface and b) a partially reduced $CeO_2$ surface. c) A stepwise reaction mechanism on oxygen reduction. g, s, lc, and $\mathbf{V_O^{\cdot\cdot}}$ represent gas, surface, lattice, and a doubly charged oxygen vacancy, respectively.

without the surface treatment by $H_2$ failed, whereas the reduced surface produced strong bands upon $O_2$ exposure, as shown in Figure 2b. The reduced $CeO_2$ surface in Ar at 298 K yields no significant signal from adsorbed oxygen species, while strong peaks at 825 and 1131 $cm^{-1}$ emerge once oxygen is introduced, implying that oxygen vacancies generated from the reduction with $H_2$ play a significant role in the formation of adsorbed species as aforementioned (see Scheme 1b). The observed adsorbed oxygen species at 825 and 1131 $cm^{-1}$ herein are quantitatively consistent with the literature values[5,9,10,20] (see Table 1). To verify that the peaks originate from an oxygen-containing species, another Raman spectrum was recorded by exposing the sample to 10% $^{18}O_2$ and observing the peak position shifts.

$CeO_2$ surfaces, implying the existence of intrinsic $Ce^{3+}$ ions. However, our first attempt to detect adsorbed oxygen species

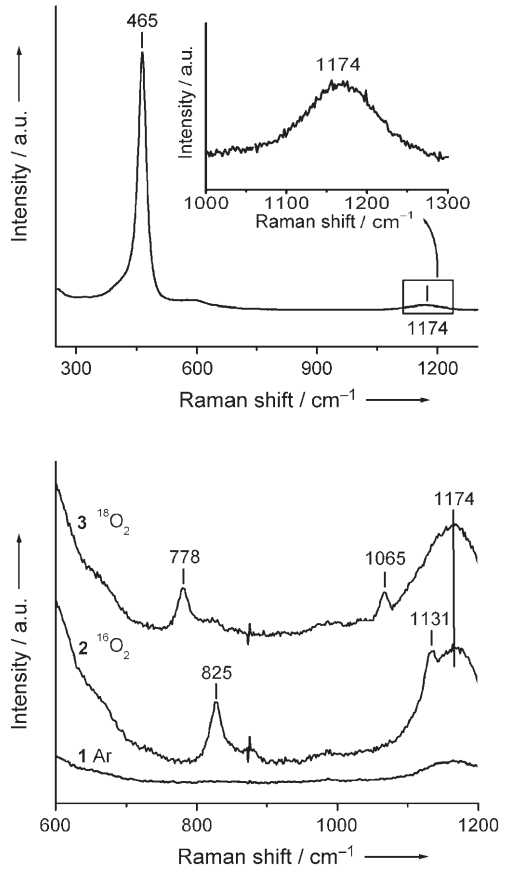


**Figure 2.** Typical Raman spectra of a) fully oxidized $CeO_2$ sample and b) $CeO_2$ sample treated with 5% $H_2$ at 673 K before 298 K exposure to 1) Ar, 2) 10% $^{16}O_2$, and 3) 10% $^{18}O_2$ atmospheres (all mixtures are diluted with Ar).

As depicted in Figure 2b and Table 1, the observed peaks at 825 and 1131 $cm^{-1}$ shift to 778 and 1065 $cm^{-1}$ with the isotopic ratios of 1.060 and 1.062, respectively, which agree with the theoretical ratio of 1.061. In addition to the high-frequency peaks (1127–1551 $cm^{-1}$), Pushkarev et al.[5] found a shift in low-frequency bands (340, 357, and 538 $cm^{-1}$ to 324, 342, and 529 $cm^{-1}$ with isotope ratios of 1.049, 1.044, and 1.017, respectively) at 93 K. Similar to the Raman data compiled in Table 1,

**Table 1.** Experimental vibrational frequencies for adsorbed oxygen species on $CeO_2$.

| $^{16}O_2$[$cm^{-1}$] | $^{18}O_2$[$cm^{-1}$] | $^{16}O_2/^{18}O_2$[a] | Remarks[b] |
|---|---|---|---|
| 1131 | 1065 | 1.062 | herein, Raman, 723 K, yes, 298 K |
| 825 | 778 | 1.060 | herein, Raman, 723 K, yes, 298 K |
| 1128 | 1064 | 1.060 | ref. [10], Raman, 723 K, yes, 298 K |
| 831 | 781 | 1.064 | ref. [10], Raman, 723 K, yes, 298 K |
| 1551 | 1465 | 1.059 | ref. [5], Raman, 673 K, yes, 93 K |
| 1487 | 1412 | 1.053 | ref. [5], Raman, 673 K, yes, 93 K |
| 1135 | 1071 | 1.060 | ref. [5], Raman, 673 K, yes, 93 K |
| 1127 | 1065 | 1.058 | ref. [5], Raman, 673 K, yes, 93 K |
| 860 | 809 | 1.063 | ref. [5], Raman, 673 K, yes, 93 K |
| 831 | 786 | 1.057 | ref. [5], Raman, 673 K, yes, 93 K |
| 538 | 529 | 1.017 | ref. [5], Raman, 673 K, yes, 93 K |
| 357 | 342 | 1.044 | ref. [5], Raman, 673 K, yes, 93 K |
| 340 | 324 | 1.049 | ref. [5], Raman, 673 K, yes, 93 K |
| 1126 | 1063 | 1.059 | ref. [9], FTIR, 1000 K, no, 298 K |
| 1128 | 1065 | 1.059 | ref. [9], FTIR, 673 K, yes, 210 K |
| 883 | 835 | 1.057 | ref. [9], FTIR, 673 K, yes, 210 K |
| 1128 | 1064 | 1.060 | ref. [20], FTIR, 673 K, no, 298–373 K |

[a] Calculated value is 1.061, $(18/16)^{1/2}$. [b] Remarks correspond to references, experimental methods, surface-pretreatment temperatures, reduced subsurface or not, and measurement temperatures, respectively.

  

the surface pretreatment for Fourier-transform infrared (FTIR) spectroscopy measurements[9,20] by $H_2$ is also very important for detecting peroxo-like species. Li and coworkers[9] reported that the intensity of a peroxo-like species at 883 $cm^{-1}$ was noticeably affected by reduction time with $H_2$ (the degree of pre-reduction by $H_2$), while the superoxo-like species at 1128 $cm^{-1}$ was slightly influenced, suggesting that surface defects play a significant role in the generation of peroxo-like species on a $CeO_2$ surface. Moreover, Zhang et al.[10] recently demonstrated that surface morphology is an important factor in observing adsorbed oxygen species. As summarized in Table 1, the observed peaks of 825–883 $cm^{-1}$ and 1126–1135 $cm^{-1}$ are attributed to peroxo- and superoxo-like species, respectively. As detailed in the following section, first-principle calculations are performed to interpret the experimental data.

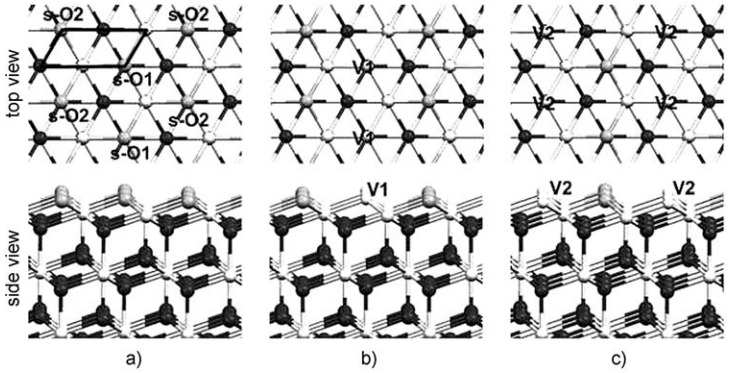


**Figure 3.** Surface models for the studies of the $O_2$–$CeO_2$(111) interactions: a), b) and c) are the unreduced and different reduced $CeO_2$(111) surfaces. Ce, subsurface oxygen and surface oxygen ions are in white, black, and gray, respectively. Oxygen vacancies are represented by **V1** and **V2**. The parallelogram in black represents a unit cell.

### 2.3. Theoretical interpretation

#### *2.3.1. Bulk Materials and Gas-Phase Oxygen*

The validity of the surface model shown in Figure 1 has been examined [14] through predictions of physical properties (i.e. lattice parameters and total density of states) that are in good agreement with available literature data. The estimated bulk lattice constant for $CeO_2$(111) of 5.419 Å agrees reasonably with the experimental value of 5.411 Å.[21] As summarized in Table 2, predicted geometrical parameters and vibrational frequencies of gas-phase $O_2$ in a 10 Å cubic box are in line with available experimental data.

**Table 2.** Geometrical parameters and vibrational frequencies of singlet and triplet $O_2$ calculated using the GGA–PAW method.

| | Calculated | | Experimental |
|---|---|---|---|
| | $^1\Delta_g$ | $^3\Sigma^-_g$ | |
| $r$(O–O) [Å] | 1.236 | 1.235 | 1.207[17] |
| $\nu_{O-O}$ [$cm^{-1}$] | 1550 | 1558 | 1550[22] |

#### *2.3.2. Surface Oxygen Intermediates on Unreduced $CeO_2$(111)*

An $O_2$ molecule was placed on various $CeO_2$(111) surface sites to initially locate possible intermediates on the unreduced $CeO_2$(111) surface (see Figure 3a). Figure 4 shows the optimized structures of adsorbed dioxygen species on the unreduced $CeO_2$(111) surface. Similar to the configurations of molecular adsorption in Scheme 1a, we found four structure types: end-on, side-on, non-planar bridging, and planar bridging (see Figure 4). Based on the geometrical configurations, they may be correlated with $\eta^1$ superoxo-, $\eta^2$ peroxo-, bridging peroxo-, and bridging superoxo-like species.[5] Table 3 compiles the adsorption energies ($0.91 < \Delta E_{ads} < 0.98$ eV) for the different molecular adsorption configurations. The highly endothermic energies may be the reason why it is difficult to detect surface

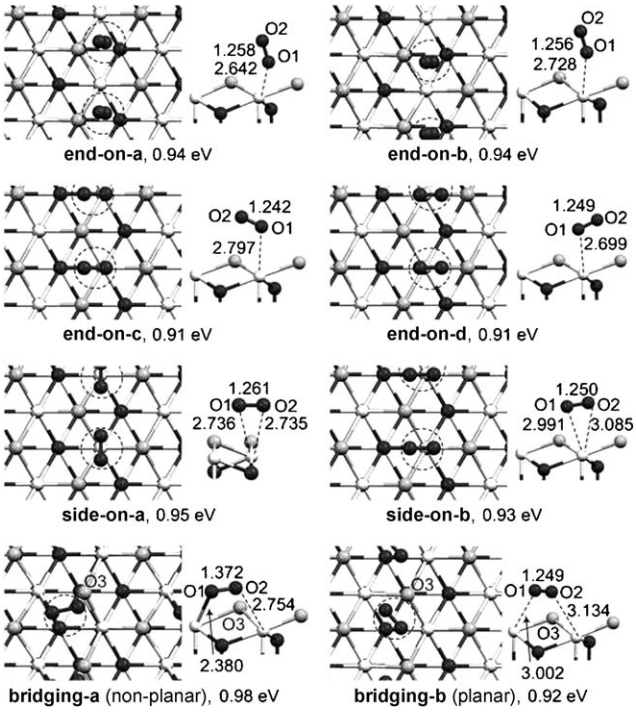


**Figure 4.** Geometrical illustration of adsorbed oxygen species at various active sites on the unreduced $CeO_2$(111) surface. Ce, subsurface oxygen and surface oxygen ions are in white, black, and gray, respectively. Dashed circles represent adsorbed oxygen species, bond lengths are in Å and the values in eV are adsorption energies between $O_2$ and the unreduced $CeO_2$(111) surface.

oxygen species on fully oxidized unreduced $CeO_2$ using vibrational spectroscopy.[10] To ensure surface relaxation effects, we also re-optimized the **end-on-a** intermediate after relaxing the top six layers. The effect is negligible on both the energetics (~4 meV) and the O–O bond distance (~0.002 Å). We briefly examined the effect of surface coverage by placing one more $O_2$ molecule onto the unit cell. This additional $O_2$ led to a slight change in the adsorption energy (+0.94 to +0.95 eV) and a decrease in the O–O bond distance (1.258 to 1.249 Å).

  

**Table 3.** Adsorption energies, geometrical parameters, predicted vibrational frequencies and partial charges (*e*) of adsorbed oxygen species on unreduced $CeO_2$(111) surface.

| Species | Adsorption energies [eV] | *r*(O–O) [Å] | $\nu_{O-O}$ [$cm^{-1}$] | *d*[a] [Å] | Partial charge O1 | O2 | Sum | Assignment[b] |
|---|---|---|---|---|---|---|---|---|
| **end-on-a** | 0.94 | 1.258 | 1383 | 1.329 | −0.16 | −0.07 | −0.23 | **W** |
| **end-on-b** | 0.94 | 1.256 | 1385 | 1.464 | −0.12 | −0.07 | −0.19 | **W** |
| **end-on-c** | 0.91 | 1.242 | 1460 | 2.046 | −0.05 | −0.03 | −0.08 | **W** |
| **end-on-d** | 0.91 | 1.249 | 1429 | 1.920 | −0.09 | −0.04 | −0.13 | **W** |
| **side-on-a** | 0.95 | 1.261 | 1383 | 1.895 | −0.08 | −0.09 | −0.17 | **W** |
| **side-on-b** | 0.93 | 1.250 | 1430 | 2.077 | −0.06 | −0.06 | −0.12 | **W** |
| **bridging-a** (non-planar) | 0.98 | 1.372 | 956 | 1.053 | −0.42 | −0.06 | −0.48 | **P** |
| **bridging-b** (planar) | 0.92 | 1.249 | 1431 | 1.876 | −0.07 | −0.07 | −0.14 | **W** |

[a] The shortest distance between the surface and adsorbed oxygen (O1 or O2) atom (see Figure 4). [b] **W** and **P** represent weakly bound physisorbed and peroxo-like species, respectively.

Partial charges of adsorbed oxygen species on the unreduced $CeO_2$(111) surface are calculated using the Bader charge analysis.[15] As compiled in Table S1, the optimized bulk structure apparently has smaller partial charges than the formal charges of Ce and O (+4 and −2 , respectively). Charge transfer from the metal-oxide surface to adsorbed oxygen species occurs, leaving the adsorbates negatively charged. The non-planar **bridging-a** configuration is the most negatively charged due to the short distance of 2.380 Å between O1 and the Ce atom, as depicted in Figure 4. Partial charges of all the atoms are summarized in Table S1 in the Supporting Information.

**Table 4.** Adsorption energies, geometrical parameters, predicted vibrational frequencies and partial charges (*e*) of adsorbed oxygen species on reduced $CeO_2$(111) surfaces.

| Species | Adsorption energies [eV] | *r*(O–O) [Å] | $\nu_{O-O}$ [$cm^{-1}$] | Partial charge O1 | O2 | Sum | Assignment[a] |
|---|---|---|---|---|---|---|---|
| **end-on-a-v1** | −4.00 | 1.426 | 972 | −0.68 | −0.49 | −1.17 | **P** |
| **end-on-a-v2** | −3.92 | 1.425 | 945 | −0.66 | −0.45 | −1.11 | **P** |
| **end-on-b-v1** | −4.00 | 1.430 | 960 | −0.68 | −0.49 | −1.17 | **P** |
| **end-on-b-v2** | −3.95 | 1.419 | 978 | −0.66 | −0.47 | −1.13 | **P** |
| **end-on-c-v1** | −0.90 | 1.314 | 1198 | −0.36 | −0.24 | −0.60 | **S** |
| **end-on-c-v2** | −0.96 | 1.329 | 1094 | −0.44 | −0.22 | −0.66 | **S** |
| **end-on-d-v1** | −1.16 | 1.330 | 1304 | −0.53 | −0.14 | −0.67 | **S** |
| **end-on-d-v2** | −3.88 | 1.425 | 936 | −0.43 | −0.66 | −1.09 | **P** |
| **side-on-a-v1** | −3.27 | 1.423 | 922 | −0.59 | −0.45 | −1.04 | **P** |
| **side-on-a-v2** | −3.54 | 1.416 | 981 | −0.47 | −0.61 | −1.08 | **P** |
| **side-on-b-v1** | −2.55 | 1.419 | 957 | −0.54 | −0.43 | −0.97 | **P** |
| **side-on-b-v2** | −3.88 | 1.425 | 934 | −0.43 | −0.66 | −1.09 | **P** |
| **bridging-a-v** | −3.95 | 1.359 | 1148 | −0.46 | −0.66 | −1.12 | **S** |
| **bridging-b-v** | −3.95 | 1.333 | 1244 | −0.65 | −0.49 | −1.14 | **S** |

[a] **S** and **P** correspond to superoxo- and peroxo-like species, respectively.

### 2.3.3. Surface Oxygen Intermediates on Reduced $CeO_2$(111) and Oxygen-Vacancy Effects

To mimic the partially reduced $CeO_2$ surface effectively by $H_2$, we artificially generated two types of oxygen vacancies, **V1** and **V2**, by removing surface oxygen anions, **s-O1** and **s-O2**, as shown in Figures 3 b and c, respectively. We assumed that a two-electron defect structure can produce more feasible surface species and account for the experimental observations discussed in the previous section. We re-optimized the geometries on the unreduced surfaces (see Figure 4) and calculated energetics and vibrational frequencies as summarized in Table 4. As illustrated in Figure 5, because of the presence of the oxygen vacancies, there is a slight structural change in the reduced surface, leaving different partial charges (see **V1** and **V2** in Table S1), especially in the top-layer atoms. In addition, the optimal geometries with the two types of oxygen vacancies, **V1** and **V2**, are significantly different, implying that oxygen-vacancy locations influence surface adsorption. According to the geometrical parameters depicted in Figure 5, after breaking the O-O bond of the adsorbed oxygen species, an O atom needs to be incorporated into or near the oxygen vacancy. Table 4 summarizes the altered O-O bonds and their vibrational frequencies. Figure 5 shows that the O-O bonds on the reduced $CeO_2$(111) surfaces vary from 1.314 to 1.430 Å, while the energetics change from −4.0 to −0.9 eV, respectively. For the partial charges, those of the bulk and the unreduced surface are very close, whereas those of the reduced surfaces, **V1** and **V2**, are noticeably changed (see Table S1). The sum of partial charges of each adsorbed oxygen species compiled in Table 4 is more negative than that on the unreduced surface in Table 3 because they have diffused into or near the oxygen vacancy. However, **end-on-c-v1**, **end-on-c-v2**, and **end-on-d-v1** have less negative partial charges due to their relatively longer O–O bond lengths. According to the comparison of the energetics between the unreduced and reduced surfaces, the reduced surfaces are energetically more favorable and produce more reasonable dioxygen species.

### 2.3.4. Comparison of Experimental and Estimated Vibrational Frequencies

To assign the experimental spectroscopic observations, we estimated the vibrational frequencies with the optimized geometries on the unreduced $CeO_2$(111) surface summarized in

  

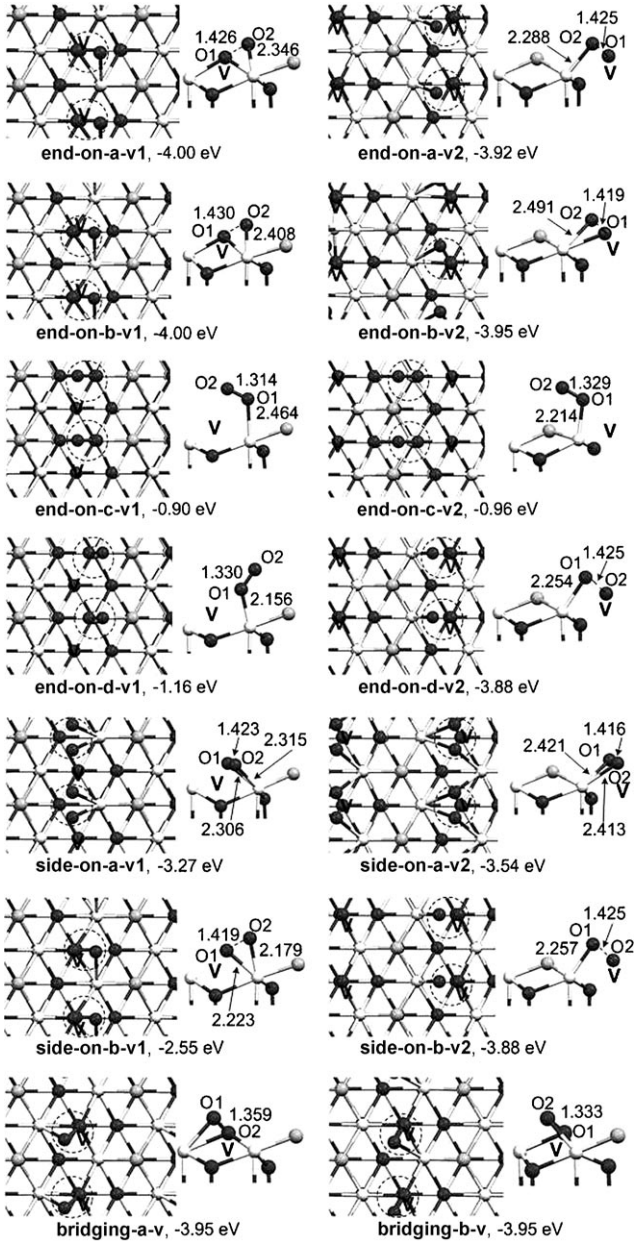


**Figure 5.** Geometrical illustration of adsorbed oxygen species on the reduced $CeO_2$(111) surfaces. Ce, subsurface oxygen and surface oxygen ions are in white, black, and gray, respectively. Dashed circles and **V** represent adsorbed oxygen species and an oxygen vacancy, respectively. Bond lengths are in Å and the values in eV are adsorption energies between $O_2$ and the reduced $CeO_2$(111) surface.

Figure 4. Table 3 compiles the predicted vibrational frequencies. It should be mentioned that correction factors for predicted harmonic vibrational frequencies are generally not available in the literature. According to the approach by Hehre and coworkers,[23] to obtain reliable correction factors for predicted harmonic vibrational frequencies, a large number of experimental values have to be applied. Due to the lack of comprehensive experimental data, we only aim for a qualitative comparison. As displayed in the Supporting Information (Figure S2), to investigate the validity of our vibrational-frequency prediction, we estimated vibrational frequencies as a function of the distance between the surface and the adsorbed dioxygen species from 1.90 to 3.90 Å,[24] corresponding to the estimated vibrational frequencies at 1392 to 1556 $cm^{-1}$, respectively. They are in good agreement with that of **side-on-a** and gas-phase $O_2$ with an uncertainty of $\approx$0.5%.

As illustrated in Figure 4, the distance between the O2 atom and the O3 surface anion of **bridging-a** is much shorter than that of planar **bridging-b** (2.754 and 3.134 Å, respectively). The relatively strong O2–O3 interaction of **bridging-a** causes a longer O1–O2 bond of 1.372 Å than that of **bridging-b**, and produces the lower frequency of 956 $cm^{-1}$, which can be qualitatively assigned to a peroxo-like species. On the other hand, the O–O bond lengths of other optimized structures are close to that of a calculated gas-phase oxygen molecule (see Table 2). Thus, we assign the predicted vibrational frequencies at 1383–1460 $cm^{-1}$ to weakly bound dioxygen intermediates observed at 1487 and 1551 $cm^{-1}$ by Pushkarev et al.,[5] as given in Table 1. To examine other possible intermediates, we introduced the oxygen vacancies described in the computational section. Figure 5 presents the configurations of **end-on-a**, end-on-b, **end-on-c**, **end-on-d**, **side-on-a**, **side-on-b**, **bridging-a**, and **bridging-a** and their derivatives produced by introducing an oxygen vacancy. The oxygen deficiency by surface reduction can alter the vibrational frequencies from those on the unreduced $CeO_2$ surface because of different equilibrium structures. For example, the O–O bond length of **end-on-c** is lengthened from 1.242 to 1.314 Å whereas the Ce–O bond distance is shortened from 2.797 to 2.464 Å, respectively, shifting the vibrational frequencies from 1460 to 1198 $cm^{-1}$, respectively. It is interesting that, regardless of the oxygen-vacancy location, an O atom of the adsorbed oxygen species on **end-on-a**, **end-on-b**, **side-on-b**, **bridging-a**, and **bridging-b** can diffuse near the oxygen vacancy. It is anticipated that this O atom can be incorporated into the oxygen vacancy as $O^{2-}$ under fuel-cell conditions.[16] Table 4 compiles the vibrational frequencies of O1–O2 for the adsorbed dioxygen species on the reduced surfaces. Based on the geometrical information and partial charges in Figure 5 and in Table 4, respectively, **end-on-c-v1**, **end-on-c-v2**, **end-on-d-v1**, **bridging-a-v**, and **bridging-b-v** are assigned to superoxo-like species, whereas **end-on-a-v1**, **end-on-a-v2**, **end-on-b-v1**, **end-on-b-v2**, **end-on-d-v2**, **side-on-a-v1**, **side-on-a-v2**, **side-on-b-v1**, and **side-on-b-v2** are attributed to peroxo-like species. The experimental bands observed at 340, 357, and 538 $cm^{-1}$ by Pushkarev et al.[5] (see Table 1) may result from highly diffused dioxygen species in oxygen vacancies.[25] A detailed mechanistic study and vibrational-frequency calculations for the oxygen-reduction reaction on a bigger $CeO_2$ surface with both unreduced and reduced active sites will be reported later.[25]

## 3. Conclusions

In situ Raman spectroscopy was used to detect dioxygen species adsorbed on $CeO_2$ at 298 K. We observed two strong peaks at 825 and 1131 $cm^{-1}$ on $CeO_2$ when it was first reduced by $H_2$ and subsequently exposed to $O_2$. These peaks are as-

  

signed to peroxo- and superoxo-like species, respectively. DFT calculations were successfully applied for the interpretation of the experimental observations. Molecular minima on the unreduced surface were initially optimized by placing an $O_2$ molecule at various active sites, with endothermic adsorption energies in the range of 0.91–0.98 eV. They were assigned to weakly physisorbed oxygen species except non-planar **bridging-a** with a vibrational frequency of 956 $cm^{-1}$. The reduction of cerium cations by the introduction of an oxygen vacancy changes the geometry and energy of the system. The dioxygen species on the reduced surfaces is attributed to the exothermic adsorption process giving peroxo- or superoxo-like species based on the geometrical parameters and partial charges. We also demonstrate that the crystallographic location of oxygen vacancies influences the formation and dissociation of adsorbed oxygen species. Furthermore, the reduced surface is energetically more favorable than the unreduced surface for oxygen reduction.

## Acknowledgements

*The authors are grateful for financial support for this work provided by the DOE-NETL-SECA core technology program (grant no. DE-FC26-02NT41572) directed by Dr. Lane Wilson. We acknowledge the use of CPUs from the National Center for High-Performance Computing, Taiwan, supported by INER under contract no. NL 940251. MCL also wants to acknowledge the support from the Taiwan National Science Council for a Distinguished Visiting Professorship at the Center for Interdisciplinary Molecular Science, National Chiao Tung University, Hsinchu, Taiwan.*

**Keywords:** adsorption · cerium · density-functional calculations · Raman spectroscopy · surface chemistry

[1] R. M. Heck, R. J. Farrauto, *Catalytic Air Pollution Control*, Van Nostrand Reinhold, New York, **1995**.
[2] a) A. Trovarelli, *Catalysis by Ceria and Related Materials*, Imperial College Press, London, **2000**; b) L. Y. Mo, X. M. Zheng, C. T. Yeh, *Chem. Commun.* **2004**, *12*, 1426; c) L. Y. Mo, X. M. Zheng, C. T. Yeh, *ChemPhysChem* **2005**, *6*, 1470.
[3] R. M. Ferrizz, G. S. Wong, T. Egami, J. M. Vohs, *Langmuir* **2001**, *17*, 2464.
[4] a) H. Inaba, H. Tagawa, *Solid State Ionics* **1996**, *83*, 1; b) F. Chen, S. Zha, J. Dong, M. Liu, *Solid State Ionics* **2004**, *166*, 269; c) C. Xia, M. Liu, *Solid State Ionics* **2001**, *144*, 249; d) C. Xia, M. Liu, *Solid State Ionics* **2002**, *152*, 423; e) S. Zha, A. Moore, H. Abernathy, M. Liu, *J. Electrochem. Soc.* **2004**, *151*, A1128; f) S. Zha, W. Rauch, M. Liu, *Solid State Ionics* **2004**, *166*, 241.
[5] V. V. Pushkarev, V. I. Kovalchuk, J. L. d'Itri, *J. Phys. Chem. B* **2004**, *108*, 5341.
[6] a) S. Gennard, F. Cora, C. Richard, A. Catlow, *J. Phys. Chem. B* **1999**, *103*, 10158; b) N. V. Skorodumova, M. Baudin, K. Hermansson, *Phys. Rev. B* **2004**, *69*, 075401; c) N. V. Skorodumova, S. I. Simak, B. I. Lundqvist, I. A. Abrikosov, B. Johansson, *Phys. Rev. Lett.* **2002**, *89*, 166601.
[7] Z. Yang, T. K. Woo, M. Baudin, K. Hermansson, *J. Chem. Phys.* **2004**, *120*, 7741.
[8] M. Liu, X. Lu, P. Faguy, *Proc. Electrochem. Soc.* **2003**, *2003-7*, 1132.
[9] a) C. Li, K. Domen, K.-i. Maruya, T. Onishi, *J. Am. Chem. Soc.* **1989**, *111*, 7683; b) C. Li, K. Domen, K.-i. Maruya, T. Onishi, *J. Catal.* **1990**, *123*, 436.
[10] Y. Zhang, Z. Kang, J. Dong, H. Abernathy, M. Liu, *J. Solid State Chem.* **2006**, *179*, 1733.
[11] M. A. Henderson, C. L. Perkins, M. H. Engelhard, S. Thevuthasan, C. H. F. Peden, *Surf. Sci.* **2003**, *526*, 1.
[12] a) G. Kresse, J. Furthmüller, *Phys. Rev. B* **1996**, *54*, 11169; b) G. Kresse, J. Hafner, *Phys. Rev. B* **1993**, *47*, 558.
[13] P. Blochl, *Phys. Rev. B* **1994**, *17*, 953.
[14] H. T. Chen, Y. M. Choi, M. Liu, M. C. Lin, unpublished results.
[15] a) G. Henkelman, A. Arnaldsson, H. Jonsson, *Comput. Mater. Sci.* **2006**, *36*, 354; b) http://theory.cm.utexas.edu/bader.
[16] N. Q. Minh, T. Takahashi, *Science and Technology of Ceramic Fuel Cells*, Elsevier, Amsterdam, **1995**.
[17] A. Bielanski, J. Haber, *Oxygen in catalysis*, Marcel Dekker, New York, **1991**.
[18] W. H. Weber, K. C. Hass, J. R. McBride, *Phys. Rev. B* **1993**, *48*, 178.
[19] A. Siokou, R. M. Nix, *J. Phys. Chem. B* **1999**, *103*, 6984.
[20] M. Haneda, T. Mizushima, N. Kakuta, *J. Chem. Soc. Faraday Trans.* **1995**, 4459.
[21] E. A. Kummerle, G. Heger, *J. Solid State Chem.* **1999**, *147*, 485.
[22] G. Herzberg, *Molecular Spectra and Molecular Structure, Vol. I—Spectra of Diatomic Molecules*, 2nd ed., Krieger, Malabar, **1950**.
[23] W. J. Hehre, L. Radom, P. v. R. Schleyer, J. A. Pople, *Ab initio molecular orbital theory*, Wiley, New York, **1986**.
[24] For this calculations, we chose the optimized geometry of **side-on-a** as an initial equilibrium structure, and varied the distance (*d*) between the $CeO_2$ surface and the adsorbed dioxygen species. The distance *d* varied from that of **side-on-a** (1.90 Å) to 3.9 Å. The predicted vibrational frequency of the **side-on-a** intermediate is 1384 $cm^{-1}$.
[25] For a mechanistic study, we constructed a bigger surface with 12 Ce and 25 O atoms in which we could introduce partially reduced active sites, $Ce^{4+}$ and $Ce^{3+}$. We found that an almost dissociated oxygen species has a weak O–O bond of 1.724 Å and a low frequency of 330 $cm^{-1}$.

Received: March 29, 2006
Revised: June 13, 2006
Published online on August 10, 2006

  